Direct radiative effect of dust-pollution interactions

Klaus Klingmüller[1], Jos Lelieveld[1,2], Vlassis A. Karydis[1,3], and Georgiy L. Stenchikov[4]

[1]Max Planck Institute for Chemistry, Hahn-Meitner-Weg 1, 55128 Mainz, Germany

[2]The Cyprus Institute, P.O. Box 27456, 1645 Nicosia, Cyprus

[3]Forschungszentrum Jülich GmbH, IEK-8, 52425 Jülich, Germany

[4]King Abdullah University of Science and Technology, Thuwal 23955-6900, Saudi Arabia

Correspondence: Klaus Klingmüller (k.klingmueller@mpic.de)

Abstract. The chemical ageing of aeolian dust, through interactions with air pollution, affects the optical and hygroscopic properties of the mineral particles and hence their atmospheric residence time and climate forcing. Conversely, the chemical composition of the dust particles and their role as coagulation partners impact the abundance of particulate air pollution. This results in an anthropogenic radiative forcing associated with mineral dust notwithstanding the natural origin of most aeolian dust. Using the atmospheric chemistry climate model EMAC with a detailed parametrisation of ageing processes and an emission scheme accounting for the chemical composition of desert soils, we study the direct radiative forcing globally and regionally. Our results indicate large positive and negative forcings, depending on the region. The predominantly negative forcing at the top of the atmosphere over large parts of the dust belt, from West Africa to East Asia, attains a maximum of about $-2 \ \mathrm{W/m^2}$ south of the Sahel, in contrast to a positive forcing over India. Globally averaged, these forcings partially counterbalance, resulting in a net negative forcing of $-0.05 \ \mathrm{W/m^2}$, which nevertheless represents a considerable fraction of the total dust forcing.

1 Introduction

Atmospheric aerosols play an important role in the climate system by affecting radiative transfer and thus the planet's energy budget, both directly by scattering and absorption and indirectly via its impact on cloud formation (IPCC, 2014). Furthermore, fine particulate matter can be a human health hazard and is a major cause of morbidity and mortality globally (Lelieveld et al., 2015).

Aerosols originate both from natural and anthropogenic sources, the former being mostly mineral dust, sea salt and emissions from naturally ignited fires. Mineral dust is the dominant aerosol component by mass and natural sources are responsible for most of its atmospheric load, even though about 25 % may be from man-made sources (Ginoux et al., 2012). The natural sources provide an inevitable background level of atmospheric particulate matter, while studies of the human impact on climate and air
5 pollution commonly focus on aerosol from anthropogenic sources. However, within the atmosphere natural and anthropogenic aerosols are mixed and interact, and therefore should not be considered separately.

In the presence of anthropogenic pollution, gaseous compounds, notably acids, condense on the mineral dust particles (Karydis et al., 2011). The consequent interactions are dubbed chemical ageing, converting the initially hydrophobic dust particles into hydrophilic ones (Karydis et al., 2017), leading to the hygroscopic growth of the particles with implications for their op-
10 tical properties and the rate of deposition (Levin et al., 1996; Abdelkader et al., 2015, 2017). The dust particles also serve as coagulation partners for particulate anthropogenic pollution. Moreover, the chemical composition of the dust particles affects the chemical properties of the aerosol mixture (Karydis et al., 2016) and hence the hygroscopic and optical properties as well as the atmospheric residence time of both the natural and anthropogenic components. In view of emerging economies with growing population and increasing emissions from industry, energy production and transport in dust affected regions such as
15 northern Africa, the Middle East and large parts of Asia, the importance of these effects is ever-increasing (Osipov et al., 2015; Osipov and Stenchikov, 2018).

In the present study we analyse the impact of mineral dust interactions with anthropogenic air pollution on radiative transfer using the ECHAM/MESSy chemistry climate model (EMAC) (Jöckel et al., 2005, 2010). EMAC combines the Modular Earth Submodel System (MESSy) with the ECMWF/Hamburg (ECHAM) climate model which is originally based on the weather
20 forecasting model of the European Centre for Medium-Range Weather Forecasts (ECMWF). Here we focus on the direct radiative effects while not considering aerosol cloud coupling, and ignoring radiative feedbacks on the climate system. Both aspects, of which especially the former influences radiative forcing, will be considered in a separate study based on climate model simulations that account for atmosphere-ocean coupling.

The article is structured as follows: In section 2 we present our methodology including the model setup-up. The effects
25 of dust-pollution interactions on the aerosol burdens and correspondingly the optical properties are analysed in section 3, the resulting impacts on radiative transfer and atmospheric heating in section 4. Conclusions are drawn in section 5.

2 Methodology

We use the EMAC model version and configuration described by Klingmüller et al. (2018), which was shown to yield realistic results of aerosol optical properties globally (see Fig. S1 in the supplement). This EMAC version combines ECHAM 5.3.02 and MESSy 2.52 and is configured to use the horizontal resolution T106 and 31 vertical levels. The grid spacing of the Gaussian T106 grid, $1.125°$ along latitudes and about $1.121°$ along longitudes, at the equator corresponds to virtually quadratic cells with around 125 km edge length. The following MESSy submodels have been enabled: AEROPT, AIRSEA, CLOUD, CLOUDOPT, CONVECT, CVTRANS, DDEP, GMXE, JVAL, LNOX, MECCA, OFFEMIS, ONEMIS, ORBIT, ORACLE, PTRAC, RAD, SCAV, SEDI, SURFACE, TNUDGE, TROPOP. Descriptions of each submodel and further references can be found online in the MESSy submodel list (MESSy 2018). The model dynamics above the boundary layer are nudged to meteorological analyses of the European Centre for Medium-Range Weather Forecasts (ECMWF), and the prognostic radiative-transfer calculation uses the Tanre aerosol climatology for extinction, single scattering albedo and asymmetry factor (Tanre et al., 1984). The aerosol radiative coupling to the meteorology, and that between aerosols and clouds have been disabled to exclude higher order effects such as feedbacks by precipitation and evaporation changes and to focus on the direct radiative forcing. The CMIP5 RCP4.5 (Coupled Model Intercomparison Project Phase 5 Representative Concentration Pathway 4.5) (Clarke et al., 2007), GFEDv3.1 (Global Fire Emissions Database) (Randerson et al., 2013) and AeroCom (Aerosol Comparisons between Observations and Models) (Dentener et al., 2006) databases provide anthropogenic, biomass burning and sea salt emissions, respectively.

The EMAC model considers dust ageing by condensation of soluble compounds, reactions into ionic species and the associated water uptake. The relevant submodels include the Global Modal Aerosol Extension (GMXE) (Pringle et al., 2010a, b), which simulates the aerosol micro-physics considering four soluble (nucleation, Aitken, accumulation, coarse) and three insoluble modes (Aitken, accumulation, coarse) employing ISORROPIA II (Fountoukis and Nenes, 2007) or EQSAM4clim (Equilibrium Simplified Aerosol Model V4 for climate simulations) (Metzger et al., 2016) for the gas-aerosol partitioning (here we use the former). The ORACLE (Organic Aerosol Composition and Evolution) submodel comprehensively describes organic aerosols (Tsimpidi et al., 2014). Aerosol optical properties are calculated by the AEROPT (AERosol OPTical properties) submodel (Lauer et al., 2007; Pozzer et al., 2012; Klingmüller et al., 2014), which assumes the aerosol components within each mode to be well mixed in spherical particles with volume averaged refractive index. The refractive indices considered for the individual components are specified in the supplement of Klingmüller et al. (2014). A detailed simulation of the gas phase chemistry is performed by the Module Efficiently Calculating the Chemistry of the Atmosphere (MECCA) (Sander et al., 2011). The dust emission scheme is evaluated within the online emission submodel ONEMIS (Kerkweg et al., 2006). We use

the dust emission scheme presented by Klingmüller et al. (2018) which is based on Astitha et al. (2012) and differentiates the Ca^{++}, K^+, Mg^{++} and Na^+ fractions in mineral particles originating from different deserts (Karydis et al., 2016).

Our analysis covers the meteorological year 2011. Four simulations with varied emission setups (Table 1) are used to derive the instantaneous forcing by the interaction of mineral dust and anthropogenic pollution: one simulation considering all emis-

5   sions (simulation 1), the same simulation but without dust emissions (simulation 2), a simulation with only natural emissions (simulation 3) and the corresponding simulation without dust emissions (simulations 4). For the natural emission setups we omit the CMIP5 anthropogenic emissions and reduce the GFED biomass burning emissions by 90 % (Levine, 2014). All dust emissions are considered to be natural, hence the anthropogenic impacts of land use and climate change on the dust emissions (Klingmüller et al., 2016) are excluded from our analysis. The contribution of dust-pollution interactions to the total aerosol

10   radiative forcing can be calculated from the aerosol forcings $F_{1...4}$ from the four simulations 1 to 4 by evaluating

$$\Delta F = (F_1 - F_2) - (F_3 - F_4), \tag{1}$$

the difference of the dust forcing with full emissions $F_1 - F_2$ and the dust forcing with only natural emissions $F_3 - F_4$. Analogously, we define the dust-pollution interaction effect on aerosol optical depth (AOD), atmospheric heating rates and aerosol particle burdens.

15   Note that the right hand side of Eq. 1 is symmetric regarding the exchange of dust and anthropogenic emissions, i.e., it considers the effect of the pollution on dust in the same way as the effect of dust on pollution. It can be instructive to expand the term to the difference of the combined dust and pollution forcing $F_1 - F_4$ and the sum of the forcing of only dust $F_2 - F_4$ and only pollution $F_3 - F_4$,

$$\Delta F = \big(F_1 - F_4\big) - \big((F_2 - F_4) + (F_3 - F_4)\big). \tag{2}$$

20   Due to clouds, radiative forcings strongly vary over time and accordingly their temporal averages are associated with substantial statistical uncertainty even for relatively long averaging intervals. Calculating the aerosol forcing as the difference between fluxes computed by two simultaneous radiative transfer computations, one with and one without considering the aerosol but both with identical cloud effect, eliminates most of the cloud related statistical noise. This drastically reduces the length of the averaging period which is required to obtain significant results.

25   To estimate the remaining statistical uncertainty, we split the time series of daily averages into n sub-samples, each consisting of only every n-th daily value. As long as the choice of n is not too large, this ensures that each sub-sample is unbiased

by seasonality. We consider the random terms of the sub-samples to be largely uncorrelated, which allows computation of the statistical uncertainty as standard error of the mean (SEM) of the results from all sub-samples. To obtain approximate uncertainty estimates, we use $n = 5$ for annual and $n = 7$ for seasonal analyses, which are small numbers with regard to the SEM calculation but ensure representative subsets and are factors of the number of days per year and season, respectively. We

5   use the resulting uncertainty estimate σ to apply a significance threshold of 2σ to our results. For our purpose, the one year simulation period turns out to be sufficient to produce significant results.

The difference between the global direct aerosol radiative forcings in simulation 2 and simulation 4 yields an anthropogenic aerosol forcing of -0.61 W/m^2 at the top of the atmosphere (TOA) (see Figs. S2 to S5 in the supplement), consistent with the estimate of the aerosol-radiation interaction effective radiative forcing (ERF) of -0.45 (-0.95 to 0.05) W/m^2 indicated by

10   IPCC (2014).

The global dust radiative forcing excluding the effect of dust-pollution interaction can be calculated as difference between the aerosol forcings in simulation 3 and simulation 4. At the TOA the net forcing amounts to -0.08 W/m^2, comprising the solar radiation forcing of -0.16 W/m^2 and the terrestrial radiation forcing of 0.09 W/m^2 (see Figs. S6 to S9 in the supplement). The net forcing is less negative than the -0.14 W/m^2 reported by (Bangalath and Stenchikov, 2015), but well within the range

15   of -0.48 to 0.20 W/m^2 estimated by Kok et al. (2017) and the wide spread of forcings from different models (Fig. S10 in the supplement, Yue et al. (2010), Table 1). The relatively small dust forcings in the present study compared to previous work suggest that our estimates for the radiative effect of dust-pollution interaction which predominantly affects the solar spectrum may be considered as conservative.

3   Aerosol burdens and optical properties

20   The condensation of soluble compounds, their reaction and the consequent hygroscopic growth increase the size of the dust particles and thereby their dry deposition velocity and the efficiency of in- and below-cloud scavenging. Figure 1 (top) shows that the anthropogenic dust ageing significantly reduces the dust and hence the coarse mode annual mean mass burden throughout most dust affected regions. The only notable exception is over the western Atlantic Ocean. After transport and mixing with African pollution, well aged Saharan dust takes up substantial amounts of water resulting in a regional increase of the coarse

25   mode burden; elsewhere the hygroscopic growth does not compensate the burden decrease due to the more efficient removal.

The effect on the accumulation mode aerosol burden, being most relevant for the AOD and hence radiative transfer, is more complex because not only the effect of pollution on dust but also the effect of dust on accumulation mode pollution is relevant. For instance, in the full emission simulation 1, unlike the dust free simulation 2, ammonium is driven out of the aerosol

phase by the mineral cations (Metzger et al., 2006), which results in reduced aerosol ammonium burdens but increased gas phase ammonia burdens (Fig. S11 in the supplement). This predominantly affects the accumulation mode which contains most ammonium. Conversely, the aerosol nitrate burdens are enhanced through the interaction of mineral cations with gas phase nitric acid. In contrast, aerosol sulphate is transferred from the accumulation mode to the coarse mode through coagulation

5   in the presence of coarse dust particles. The changes of the accumulation mode composition reduce the hygroscopicity, the amount of accumulation mode water and the AOD. This also prolongs the atmospheric residence time of accumulation mode pollution particles in the full emission simulation 1 compared to the dust free simulation 2, increasing the burden. In comparison with the pollution free simulation 3, the accumulation mode burden is enhanced by the reduced coagulation with coarse mode dust particles which are more efficiently removed in the presence of pollution (Fig. S12 in the supplement). In our simulation,

10   the effects that increase the accumulation mode burden generally outweigh the decrease due to more efficient deposition of accumulation mode dust particles. As shown in Fig. 1 (bottom), the interaction of anthropogenic pollution and dust results in an increased annual mean accumulation mode burden over most regions. Only over some regions, most notably over Tibet, the decreased amount of accumulation mode water results in a decreased total aerosol burden (Fig. S13 in the supplement).

The net depleting effect of dust-pollution interactions on the coarse mode aerosol burden reduces the coarse mode con-

15   tribution to the AOD, but the total AOD in the solar spectrum is dominated by the accumulation mode which is enhanced. Indeed, the annual mean effect on the AOD distribution depicted at the top of Fig. 2 clearly resembles that of the effect on the accumulation mode shown at the bottom of Fig. 1 (Fig. 2 shows the AOD for the EMAC shortwave band from 250 to 690 nm including the visible wavelengths, the effect on the 550 nm AOD is practically identical, see Fig. S14 in the supplement).

The effect on the aerosol absorption optical depth (AAOD) shown at the bottom of Fig. 2 is slightly negative, due to the

20   higher reflectance and more efficient removal of aged hygroscopic coarse mode dust. Only south of the Sahel, where the Saharan dust mixes with biomass burning pollution, the AAOD is increased due to the strong AOD increase.

The generally reduced absorption by mineral dust interacting with pollution is also reflected in larger single scattering albedos (SSA) over dust dominated regions in simulation 1 compared to simulation 3 without anthropogenic emissions. Fig. 3 shows the annual mean difference of the SSA in both simulations. The SSA values have been averaged over the vertical

25   levels weighted with the extinction, corresponding to using $SSA = 1 - AAOD/AOD$. Although carbonaceous components of the anthropogenic pollution reduce the SSA over the remaining globe, over the dust belt the SSA increases by up to 0.01. Together with the uncertainty of the refractive index of mineral dust, neglecting this SSA increase might be responsible for an overestimation of the atmospheric heating by dust (Balkanski et al., 2007). In the terrestrial spectrum aerosol particles are strongly absorbing corresponding to very small SSA values which are approximated by zero in the terrestrial radiative transfer

code. Therefore, unlike the solar radiation, the terrestrial radiation is affected by the dust-pollution interaction only via the modified extinction.

4   Radiative forcings and heating rates

The increased AOD and decreased solar radiation absorption due to dust-pollution interactions result in a predominantly negative instantaneous direct top of the atmosphere (TOA) forcing, illustrated in Fig. 4 (top). The consequent climate cooling tendency affects large parts of the dust belt, from West Africa to East Asia, and attains an annual average of about $-2 \, \mathrm{W/m^2}$ south of the Sahel. Positive forcings occur over Asia, exceeding $0.5 \, \mathrm{W/m^2}$ over India.

The distribution of the bottom of the atmosphere (BOA) forcing (Fig. 4, bottom) is similar to the that of the TOA forcing, with an annual mean cooling maximum south of the Sahel up to about $-2.5 \, \mathrm{W/m^2}$ and a warming maximum over the Indo-Gangetic Plain exceeding $1 \, \mathrm{W/m^2}$.

Consequently, the net atmospheric forcing is not very large, consistent with the moderate effect on the AAOD, but significant (Fig. 4, centre), and depending on the region can be either negative or positive. The largest region with atmospheric cooling extends from the Sahara over the Middle East to India, reaching an annual mean of $-0.8 \, \mathrm{W/m^2}$ over the Arabian Peninsula. Also over the equatorial Atlantic the dust-pollution interactions result in weak but significant atmospheric cooling. In contrast, south of the Sahel the AAOD increase (see Fig. 2) results in a positive atmospheric forcing up to $0.5 \, \mathrm{W/m^2}$. Over extensive regions in Asia, the forcing is positive as well, but mostly below $0.2 \, \mathrm{W/m^2}$.

The TOA and BOA forcings are dominated by the effect on solar radiation (shortwave, SW, Fig. S17 in the supplement). The effect on the terrestrial radiation (longwave, LW, Fig. S18 in the supplement) contributes a forcing which is one order of magnitude smaller than the SW forcing, both globally and regionally. For the atmospheric forcing, the LW contribution is more relevant and depending on the region partially compensates or enhances the SW forcing. For example, the SW heating south of the Sahel and the SW cooling west of the Red Sea are reduced by about 30 %, whereas over the Arabian Peninsula the cooling is enhanced by about 10 %.

Through atmospheric heating and cooling dust-pollution interactions may impact regional atmospheric dynamics. In Fig. 5 we analyse the heating rates in the main regions with negative (regions 1 and 2) and positive (regions 3 and 4) annual mean atmospheric forcing. Over the largest region with net atmospheric cooling, extending from the Sahara over the Middle East to India (region 1), the heating rates show little seasonal variation with a persistent cooling, which reaches a summertime average of $-0.05 \, \mathrm{K/day}$ over the Arabian Peninsula, with a minimum during winter. Similarly, the heating over the largest region with

atmospheric warming, extending from the Sahel to the Congo Basin (region 4), decreases during winter when it turns negative below 3000 m altitude.

In contrast, over regions 2 and 3 the annual average cooling and heating are largest during one season: over the equatorial Atlantic Ocean (region 2) the strongest cooling occurs during winter. Likewise, the heating over Asia is predominant during summer.

Generally, the heating takes place at higher altitudes than the cooling, at times simultaneously, thus stabilising the atmosphere, which is further intensified by the predominantly negative BOA forcing that cools the surface.

When globally averaged, the regionally positive and negative forcings partially counterbalance. Nevertheless, the net annual average global forcing at the TOA is -0.05 W/m^2, representing a considerable fraction of the total dust forcing: Fig. 6 compares this forcing with that of the dust when neglecting dust-pollution interactions, i.e., the dust forcing in the pollution free scenario $F_{\text{dust}} = F_3 - F_4$ which amounts to -0.08 W/m^2, and the dust forcing including the pollution effects, $F_{\text{dust}} = F_1 - F_2$, of -0.13 W/m^2. It is therefore recommended to take the interactions of dust and anthropogenic pollution into account when assessing the dust radiative forcing as they significantly enhance the net global climate cooling effect of mineral dust.

5   Conclusions

The physicochemical interactions of mineral dust with air pollution significantly affect the optical properties, hygroscopicity and atmospheric residence time of dust as well as anthropogenic aerosol particles. This causes an anthropogenic climate forcing linked to mineral dust, even though most of the dust itself is emitted from natural sources. Competing effects on the aerosol optical properties are involved, predominantly increasing the AOD and decreasing the AAOD.

The resulting climate forcings are non-uniformly spatially distributed with regionally large positive and negative values. The regionally negative surface forcing attains an annual mean of -2.5 W/m^2 south of the Sahel, in contrast to a mean positive forcing of 1 W/m^2 over the Indo-Gangetic Plain. The TOA forcing follows a similar pattern with slightly lower absolute values. These forcings are associated with regionally and seasonally varying atmospheric cooling and heating, with persistent cooling over large parts of the dust belt from North Africa, the Arabian Peninsula to Pakistan, and heating south of the Sahel, so that a mostly stabilising impact on the atmospheric stratification is expected, which may affect the atmospheric dynamics.

Globally, dust-pollution interactions enhance the net cooling effect of mineral dust on climate. The global, annual average TOA direct radiative forcing of -0.05 W/m^2 is of similar magnitude as the total dust forcing, which underscores the importance of a detailed account of these interactions in the assessment of aerosol radiative forcing.

To obtain the direct forcing and to reduce the statistical noise, in the present study we have excluded feedbacks of dust and other aerosol effects on radiation transfer and clouds. These are expected to have a significant impact on atmospheric dynamics and climate, which will be the subject of a subsequent study.

Code and data availability. The Modular Earth Submodel System (MESSy) is continuously further developed and applied by a consortium

5 of institutions. The usage of MESSy and access to the source code is licenced to all affiliates of institutions which are members of the MESSy Consortium. Institutions can become a member of the MESSy Consortium by signing the MESSy Memorandum of Understanding. More information can be found on the MESSy Consortium Website (https://www.messy-interface.org). The ECHAM climate model is available to the scientific community under the MPI-M Software License Agreement (https://www.mpimet.mpg.de/en/science/models/license). The simulation results analysed in this study are archived at the German Climate Computing Centre (DKRZ) and available from the corresponding

10 author KK until they are deposited in a public data repository.

Author contributions. KK performed the simulations assisted by VAK, analysed the model output and wrote the manuscript with support from JL who initiated the study. All authors interpreted the results and finalised the manuscript.

Competing interests. The authors declare that they have no conflict of interest.

Acknowledgements. The research reported in this publication has received funding from the King Abdullah University of Science and

15 Technology (KAUST) CRG3 grant URF/1/2180-01 *Combined Radiative and Air Quality Effects of Anthropogenic Air Pollution and Dust over the Arabian Peninsula.*

References

Abdelkader, M., Metzger, S., Mamouri, R. E., Astitha, M., Barrie, L., Levin, Z., and Lelieveld, J.: Dust–air pollution dynamics over the eastern Mediterranean, Atmospheric Chemistry and Physics, 15, 9173–9189, https://doi.org/10.5194/acp-15-9173-2015, 2015.

Abdelkader, M., Metzger, S., Steil, B., Klingmüller, K., Tost, H., Pozzer, A., Stenchikov, G., Barrie, L., and Lelieveld, J.: Sensitivity of
5   transatlantic dust transport to chemical aging and related atmospheric processes, Atmospheric Chemistry and Physics, 17, 3799–3821, https://doi.org/10.5194/acp-17-3799-2017, 2017.

Astitha, M., Lelieveld, J., Abdel Kader, M., Pozzer, A., and de Meij, A.: Parameterization of dust emissions in the global atmospheric chemistry-climate model EMAC: impact of nudging and soil properties, Atmospheric Chemistry and Physics, 12, 11 057–11 083, https://doi.org/10.5194/acp-12-11057-2012, 2012.

10   Balkanski, Y., Schulz, M., Claquin, T., and Guibert, S.: Reevaluation of Mineral aerosol radiative forcings suggests a better agreement with satellite and AERONET data, Atmospheric Chemistry and Physics, 7, 81–95, https://doi.org/10.5194/acp-7-81-2007, 2007.

Bangalath, H. K. and Stenchikov, G.: Role of dust direct radiative effect on the tropical rain belt over Middle East and North Africa: A high-resolution AGCM study, Journal of Geophysical Research: Atmospheres, 120, 4564–4584, https://doi.org/10.1002/2015JD023122, 2015.

15   Clarke, L. E., Edmonds, J. A., Jacoby, H. D., Pitcher, H. M., Reilly, J. M., and Richels, R. G.: Scenarios of Greenhouse Gas Emissions and Atmospheric Concentrations. Sub-report 2.1A of Synthesis and Assessment Product 2.1 by the U.S. Climate Change Science Program and the Subcommittee on Global Change Research, 2007.

Dentener, F., Kinne, S., Bond, T., Boucher, O., Cofala, J., Generoso, S., Ginoux, P., Gong, S., Hoelzemann, J. J., Ito, A., Marelli, L., Penner, J. E., Putaud, J.-P., Textor, C., Schulz, M., van der Werf, G. R., and Wilson, J.: Emissions of primary aerosol and precursor gases in the
20   years 2000 and 1750 prescribed data-sets for AeroCom, Atmospheric Chemistry and Physics, 6, 4321–4344, https://doi.org/10.5194/acp-6-4321-2006, https://www.atmos-chem-phys.net/6/4321/2006/, 2006.

Fountoukis, C. and Nenes, A.: ISORROPIA II: a computationally efficient thermodynamic equilibrium model for K^+-Ca^{2+}-Mg^{2+}-NH_4^+-Na^+-SO_4^{2-}-NO_3^--Cl^--H_2O aerosols, Atmospheric Chemistry and Physics, 7, 4639–4659, https://doi.org/10.5194/acp-7-4639-2007, http://www.atmos-chem-phys.net/7/4639/2007/, 2007.

25   Ginoux, P., Prospero, J. M., Gill, T. E., Hsu, N. C., and Zhao, M.: Global-scale attribution of anthropogenic and natural dust sources and their emission rates based on MODIS Deep Blue aerosol products, Reviews of Geophysics, 50, RG3005–, https://doi.org/10.1029/2012RG000388, 2012.

IPCC, ed.: Climate Change 2013 – The Physical Science Basis, Cambridge University Press, http://dx.doi.org/10.1017/CBO9781107415324, cambridge Books Online, 2014.

Jöckel, P., Sander, R., Kerkweg, A., Tost, H., and Lelieveld, J.: Technical Note: The Modular Earth Submodel System (MESSy) - a new approach towards Earth System Modeling, Atmospheric Chemistry and Physics, 5, 433–444, https://doi.org/10.5194/acp-5-433-2005, 2005.

Jöckel, P., Kerkweg, A., Pozzer, A., Sander, R., Tost, H., Riede, H., Baumgaertner, A., Gromov, S., and Kern, B.: Development cycle 2 of the Modular Earth Submodel System (MESSy2), Geoscientific Model Development, 3, 717, https://doi.org/10.5194/gmd-3-717-2010, 2010.

Karydis, V. A., Tsimpidi, A. P., Lei, W., Molina, L. T., and Pandis, S. N.: Formation of semivolatile inorganic aerosols in the Mexico City Metropolitan Area during the MILAGRO campaign, Atmospheric Chemistry and Physics, 11, 13 305–13 323, https://doi.org/10.5194/acp-11-13305-2011, https://www.atmos-chem-phys.net/11/13305/2011/, 2011.

Karydis, V. A., Tsimpidi, A. P., Pozzer, A., Astitha, M., and Lelieveld, J.: Effects of mineral dust on global atmospheric nitrate concentrations, Atmospheric Chemistry and Physics, 16, 1491–1509, https://doi.org/10.5194/acp-16-1491-2016, 2016.

Karydis, V. A., Tsimpidi, A. P., Bacer, S., Pozzer, A., Nenes, A., and Lelieveld, J.: Global impact of mineral dust on cloud droplet number concentration, Atmospheric Chemistry and Physics, 17, 5601–5621, https://doi.org/10.5194/acp-17-5601-2017, https://www.atmos-chem-phys.net/17/5601/2017/, 2017.

Kerkweg, A., Sander, R., Tost, H., and Jöckel, P.: Technical note: Implementation of prescribed (OFFLEM), calculated (ONLEM), and pseudo-emissions (TNUDGE) of chemical species in the Modular Earth Submodel System (MESSy), Atmospheric Chemistry and Physics, 6, 3603–3609, https://doi.org/10.5194/acp-6-3603-2006, https://www.atmos-chem-phys.net/6/3603/2006/, 2006.

Klingmüller, K., Steil, B., Brühl, C., Tost, H., and Lelieveld, J.: Sensitivity of aerosol radiative effects to different mixing assumptions in the AEROPT 1.0 submodel of the EMAC atmospheric-chemistry–climate model, Geoscientific Model Development, 7, 2503–2516, https://doi.org/10.5194/gmd-7-2503-2014, https://www.geosci-model-dev.net/7/2503/2014/, 2014.

Klingmüller, K., Pozzer, A., Metzger, S., Stenchikov, G. L., and Lelieveld, J.: Aerosol optical depth trend over the Middle East, Atmospheric Chemistry and Physics, 16, 5063–5073, https://doi.org/10.5194/acp-16-5063-2016, https://www.atmos-chem-phys.net/16/5063/2016/, 2016.

Klingmüller, K., Metzger, S., Abdelkader, M., Karydis, V. A., Stenchikov, G. L., Pozzer, A., and Lelieveld, J.: Revised mineral dust emissions in the atmospheric chemistry–climate model EMAC (MESSy 2.52 DU_Astitha1 KKDU2017 patch), Geoscientific Model Development, 11, 989–1008, https://doi.org/10.5194/gmd-11-989-2018, https://www.geosci-model-dev.net/11/989/2018/, 2018.

Kok, J. F., Ridley, D. A., Zhou, Q., Miller, R. L., Zhao, C., Heald, C. L., Ward, D. S., Albani, S., and Haustein, K.: Smaller desert dust cooling effect estimated from analysis of dust size and abundance, Nature Geoscience, 10, 274–278, https://doi.org/10.1038/ngeo2912, 2017.

Lauer, A., Eyring, V., Hendricks, J., Jöckel, P., and Lohmann, U.: Global model simulations of the impact of ocean-going ships on aerosols, clouds, and the radiation budget, Atmospheric Chemistry and Physics, 7, 5061–5079, https://doi.org/10.5194/acp-7-5061-2007, https://www.atmos-chem-phys.net/7/5061/2007/, 2007.

Lelieveld, J., Evans, J. S., Fnais, M., Giannadaki, D., and Pozzer, A.: The contribution of outdoor air pollution sources to premature mortality on a global scale, Nature, 525, 367–371, https://doi.org/10.1038/nature15371, 2015.

Levin, Z., Ganor, E., and Gladstein, V.: The Effects of Desert Particles Coated with Sulfate on Rain Formation in the Eastern Mediterranean., Journal of Applied Meteorology, 35, 1511–1523, https://doi.org/10.1175/1520-0450(1996)035<1511:TEODPC>2.0.CO;2, 1996.

Levine, J.: 5.5 - Biomass Burning: The Cycling of Gases and Particulates from the Biosphere to the Atmosphere, in: Treatise on Geochemistry (Second Edition), edited by Holland, H. D. and Turekian, K. K., pp. 139 – 150, Elsevier, Oxford, second edition edn., https://doi.org/https://doi.org/10.1016/B978-0-08-095975-7.00405-8, http://www.sciencedirect.com/science/article/pii/B9780080959757004058, 2014.

MESSy 2018: MESSy submodel list, http://www.messy-interface.org/current/auto/messy_submodels.html, visited 1 April 2018.

Metzger, S., Mihalopoulos, N., and Lelieveld, J.: Importance of mineral cations and organics in gas-aerosol partitioning of reactive nitrogen compounds: case study based on MINOS results, Atmospheric Chemistry and Physics, 6, 2549–2567, https://doi.org/10.5194/acp-6-2549-2006, https://www.atmos-chem-phys.net/6/2549/2006/, 2006.

Metzger, S., Steil, B., Abdelkader, M., Klingmüller, K., Xu, L., Penner, J. E., Fountoukis, C., Nenes, A., and Lelieveld, J.: Aerosol water parameterisation: a single parameter framework, Atmospheric Chemistry and Physics, 16, 7213–7237, https://doi.org/10.5194/acp-16-7213-2016, http://www.atmos-chem-phys.net/16/7213/2016/, 2016.

Osipov, S. and Stenchikov, G.: Simulating the Regional Impact of Dust on the Middle East Climate and the Red Sea, Journal of Geophysical Research: Oceans, 123, 1032–1047, https://doi.org/10.1002/2017JC013335, 2018.

Osipov, S., Stenchikov, G., Brindley, H., and Banks, J.: Diurnal cycle of the dust instantaneous direct radiative forcing over the Arabian Peninsula, Atmospheric Chemistry and Physics, 15, 9537–9553, https://doi.org/10.5194/acp-15-9537-2015, 2015.

Pozzer, A., de Meij, A., Pringle, K. J., Tost, H., Doering, U. M., van Aardenne, J., and Lelieveld, J.: Distributions and regional budgets of aerosols and their precursors simulated with the EMAC chemistry-climate model, Atmospheric Chemistry and Physics, 12, 961–987, https://doi.org/10.5194/acp-12-961-2012, https://www.atmos-chem-phys.net/12/961/2012/, 2012.

Pringle, K. J., Tost, H., Message, S., Steil, B., Giannadaki, D., Nenes, A., Fountoukis, C., Stier, P., Vignati, E., and Lelieveld, J.: Description and evaluation of GMXe: a new aerosol submodel for global simulations (v1), Geoscientific Model Development, 3, 391, https://doi.org/10.5194/gmd-3-391-2010, 2010a.

Pringle, K. J., Tost, H., Metzger, S., Steil, B., Giannadaki, D., Nenes, A., Fountoukis, C., Stier, P., Vignati, E., and Lelieveld, J.: Corrigendum to "Description and evaluation of GMXe: a new aerosol submodel for global simulations (v1)" published in Geosci. Model Dev., 3, 391-412, 2010, Geoscientific Model Development, 3, 413, https://doi.org/10.5194/gmd-3-413-2010, 2010b.

Randerson, J., van der Werf, G., Giglio, L., Collatz, G., and Kasibhatla, P.: Global Fire Emissions Database, Version 3 (GFEDv3.1), https://doi.org/10.3334/ORNLDAAC/1191, 2013.

Sander, R., Baumgaertner, A., Gromov, S., Harder, H., Jöckel, P., Kerkweg, A., Kubistin, D., Regelin, E., Riede, H., Sandu, A., Taraborrelli, D., Tost, H., and Xie, Z.-Q.: The atmospheric chemistry box model CAABA/MECCA-3.0, Geoscientific Model Development, 4, 373–380, https://doi.org/10.5194/gmd-4-373-2011, https://www.geosci-model-dev.net/4/373/2011/, 2011.

Tanre, D., Geleyn, J.-F., and Slingo, J. M.: First results of the introduction of an advanced aerosol-radiation interaction in the ECMWF low resolution global model, in: Aerosols and their climatic effects, edited by Gerber, H. and Deepak, A., pp. 133–177, A. Deepak Pub., 1984.

Tsimpidi, A. P., Karydis, V. A., Pozzer, A., Pandis, S. N., and Lelieveld, J.: ORACLE (v1.0): module to simulate the organic aerosol composition and evolution in the atmosphere, Geoscientific Model Development, 7, 3153–3172, https://doi.org/10.5194/gmd-7-3153-2014, https://www.geosci-model-dev.net/7/3153/2014/, 2014.

Yue, X., Wang, H., Liao, H., and Fan, K.: Direct climatic effect of dust aerosol in the NCAR Community Atmosphere Model Version 3 (CAM3), Advances in Atmospheric Sciences, 27, 230–242, https://doi.org/10.1007/s00376-009-8170-z, 2010.

Δ coarse mode burden
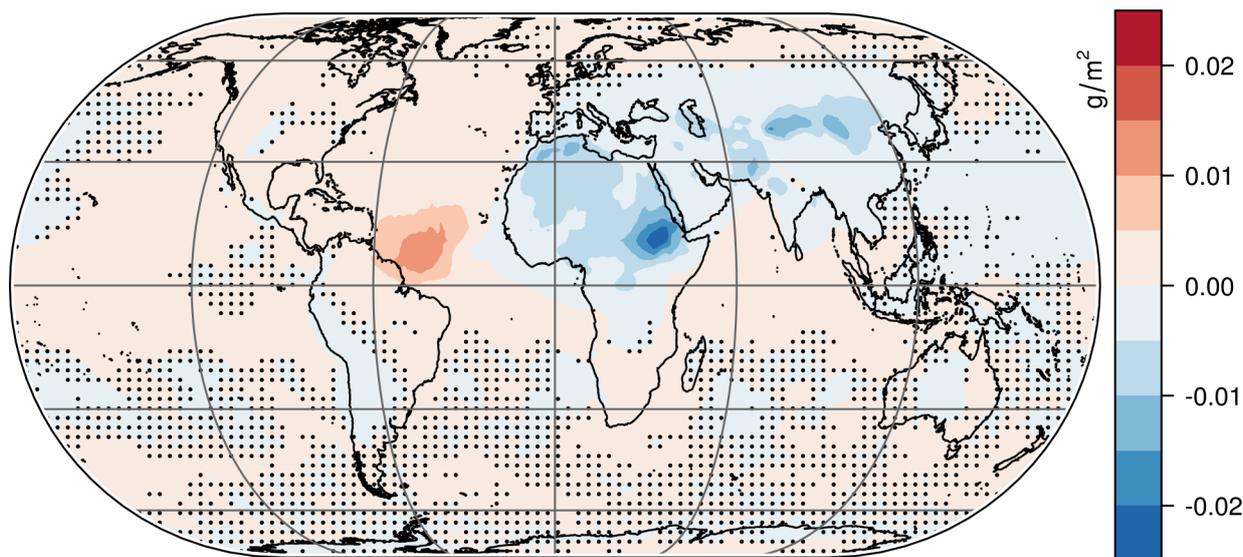
Δ accumulation mode burden
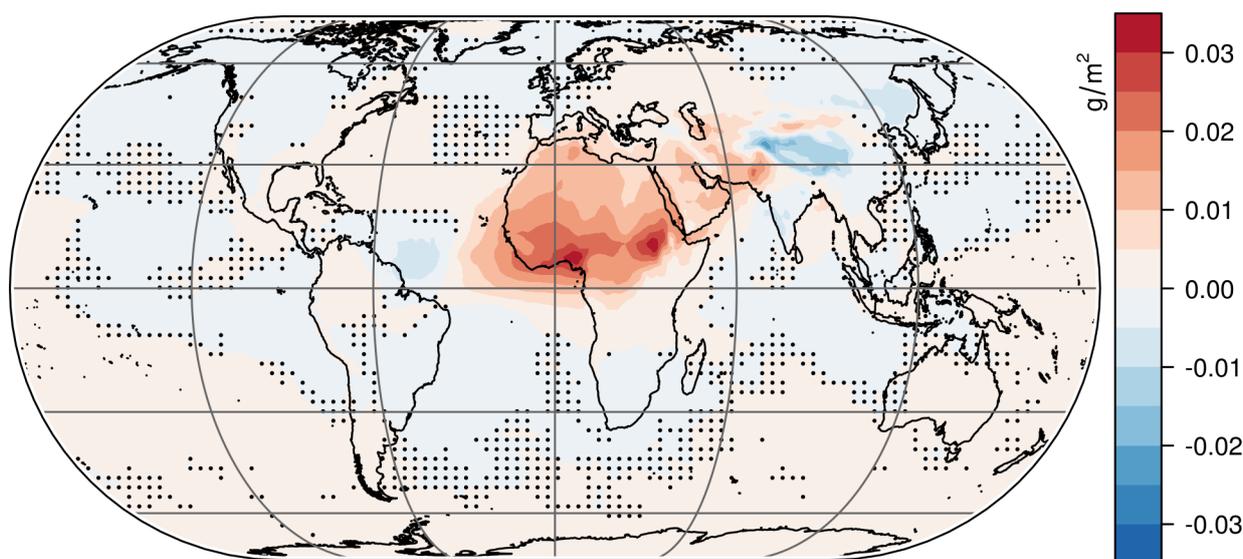
Figure 1. Impact of dust-pollution interaction on the coarse mode (top) and accumulation mode (bottom) aerosol burden. The more efficient removal of aged dust particles reduces the coarse mode burden throughout the dust belt. This in turn reduces the coagulation efficiency of coarse mode with smaller particles, increasing the accumulation mode burden especially where the dust and the African biomass burning regions coincide. The strong hygroscopic growth of aged Saharan dust particles over the western Atlantic results in a regional maximum of the coarse mode burden increase. Generally, the hygroscopic growth of accumulation mode particles is reduced by the interaction with mineral dust cations manifested in a decreased accumulation mode burden over Tibet. Dots indicate regions where the effect of the dust-pollution interaction is insignificant.

ΔAOD (250 to 690 nm)

ΔAAOD (250 to 690 nm)
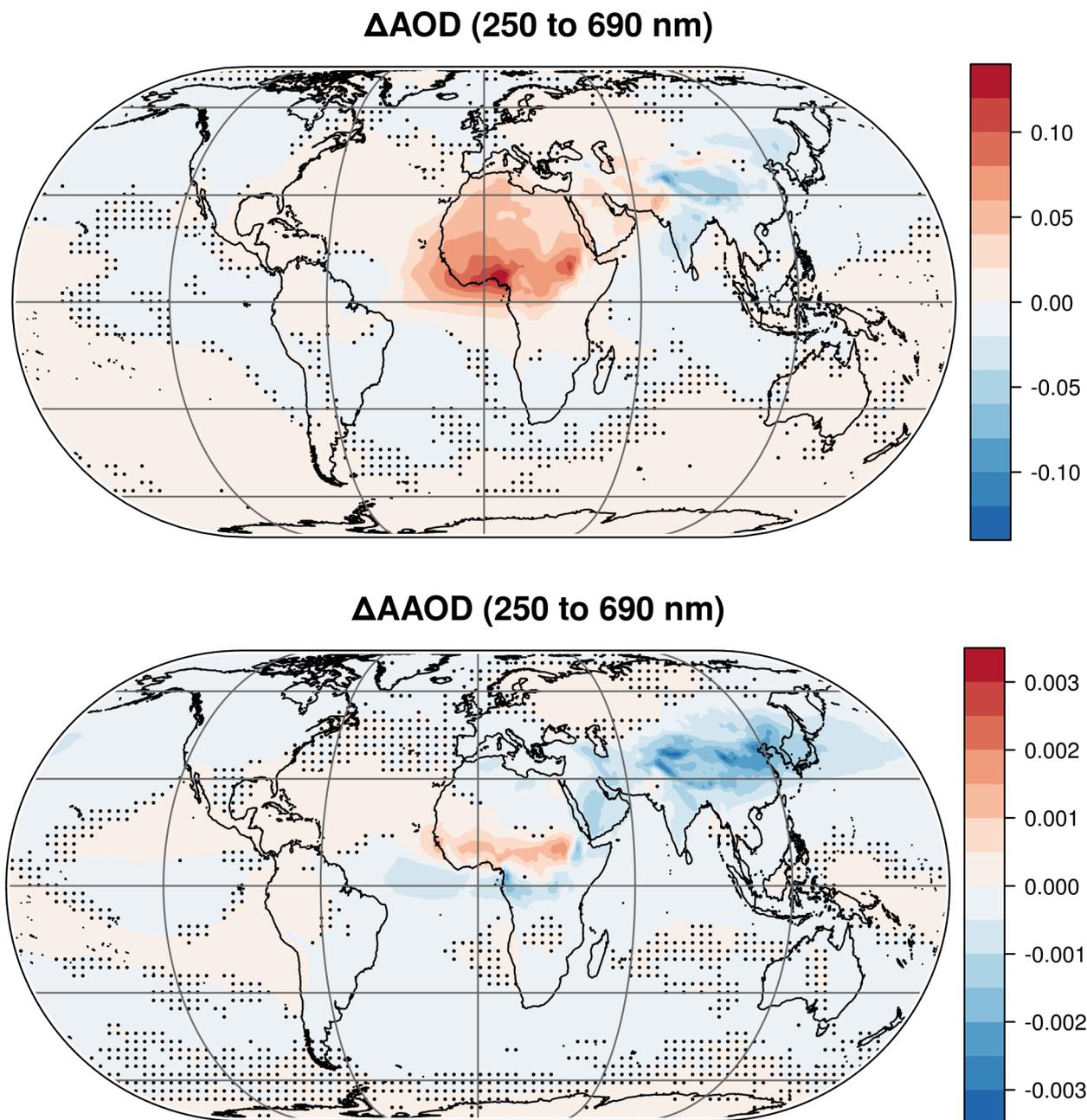
Figure 2. Impact of dust-pollution interaction on the AOD (top) and the absorption AOD (AAOD, bottom). The AOD change reflects the changes of the accumulation mode burden shown in Fig. 1. Over large parts of the dust belt the accumulation mode AOD is increased. In contrast, over the Tibetan Plateau and east India the AOD decreases due to reduced hygroscopic growth of accumulation mode particles. South of the Sahel, where the Saharan dust mixes with biomass burning pollution, the strongest accumulation mode AOD and AAOD increase occurs. Elsewhere, the water uptake of dust and the more efficient removal of absorbing coarse dust particles combined with the changed accumulation mode paricle radii and refractive indices tend to decrease the AAOD. Dots indicate regions where the effect of the dust-pollution interaction is insignificant. Figure S15 in the supplement shows the corresponding plots for the four seasons.

ΔSSA (with - without pollution) (250 to 690 nm)
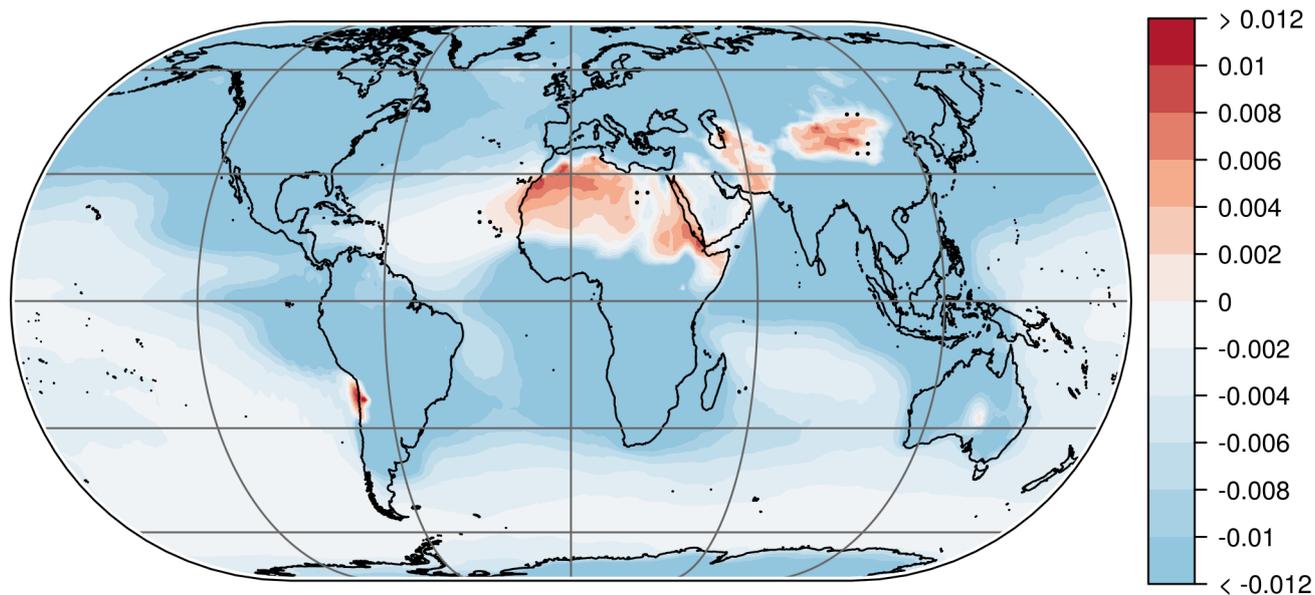
Figure 3. Annual mean difference of the single scattering albedo (SSA) with (simulation 1) and without (simulation 3) anthropogenic emissions. Extinction weighted mean SSA values of each vertical column are used. The SSA for all four emission setups is shown in Fig. S16 in the supplement. Dots indicate regions where the difference is insignificant.
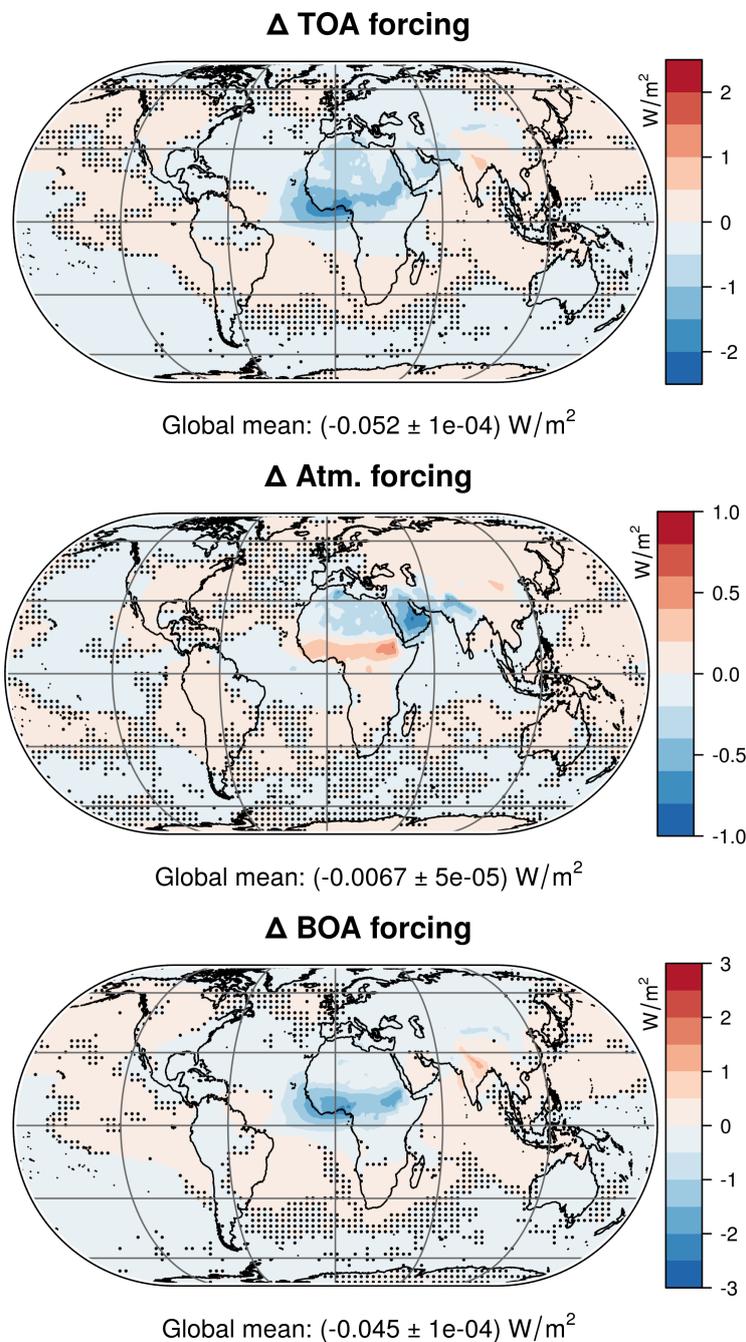
Figure 4. The instantaneous total (solar and terrestrial) direct radiative forcing of the dust-pollution interaction at the top of the atmosphere (TOA, top), within the atmosphere (centre) and at the bottom of the atmosphere (BOA, bottom). Dots indicate regions where the effect of the dust-pollution interaction is insignificant. The corresponding figures showing the solar and terrestrial forcings as well as seasonality are provided in the supplement (Figs. S17 to S19).
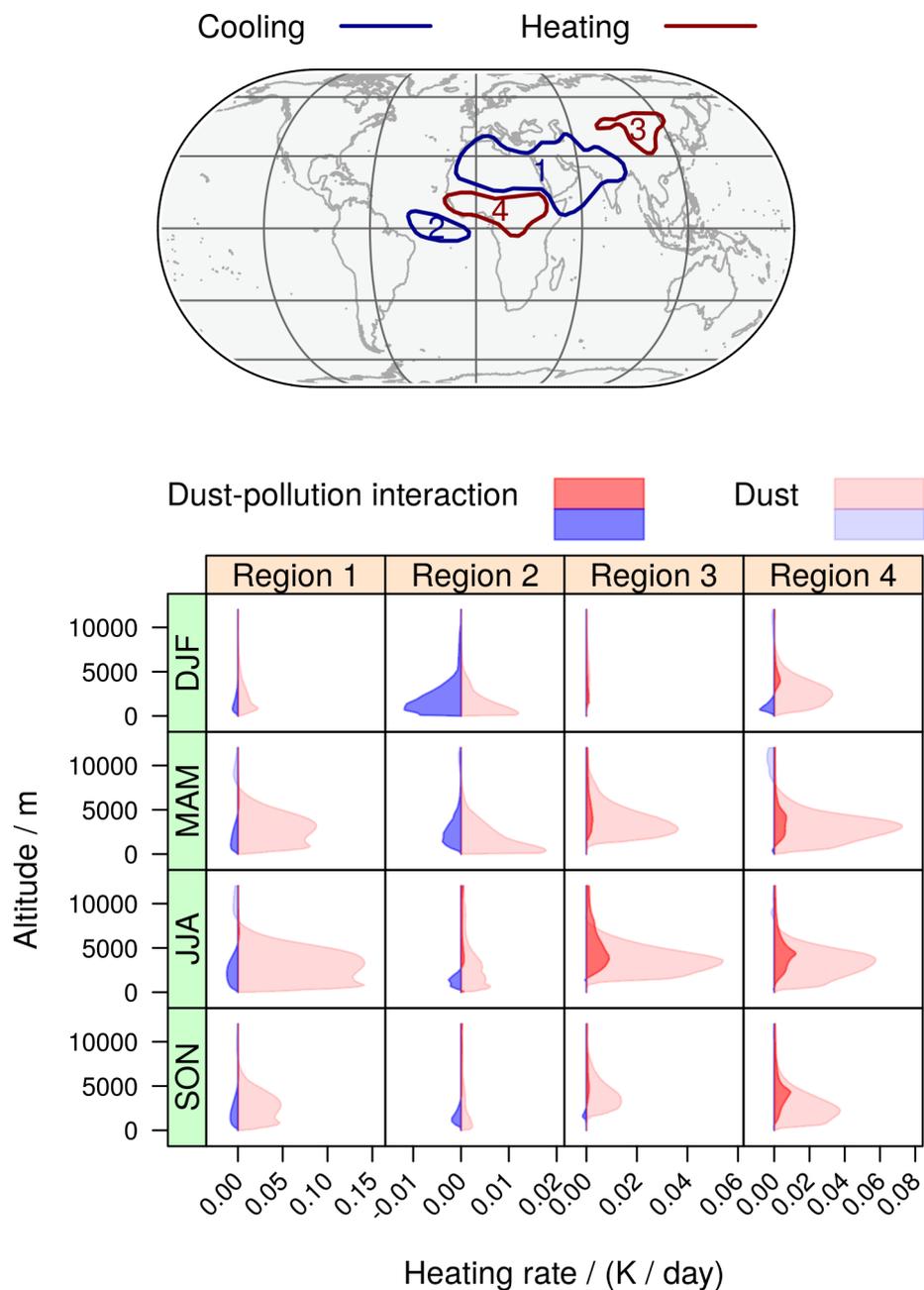
Figure 5. Heating rate contribution of dust-pollution interaction in comparison with the mineral dust contribution. Seasonal heating rate profiles of four regions with negative (regions 1 and 2) and positive (regions 3 and 4) annual mean atmospheric forcing are shown (bottom). The regions (top) are selected based on the forcings displayed in the centre of Fig. 4, using regions where the absolute forcing exceeds $0.1\,\mathrm{W/m^2}$ after applying a Gaussian filter to avoid fragmentation. Three-dimensional isosurfaces of the seasonal heating rates are presented in the supplement (Figs. S20 to S23).
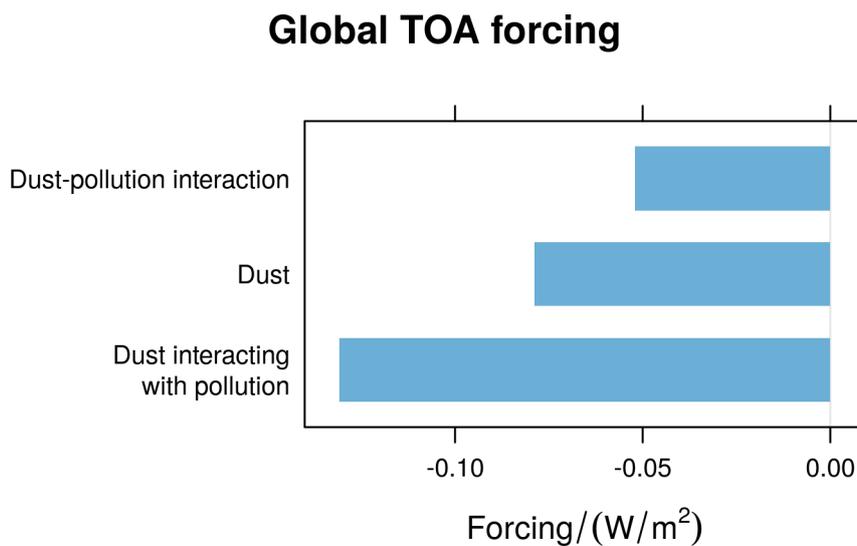
Figure 6. Global mean top of the atmosphere (TOA) forcing of the dust-pollution interaction in comparison with the mineral dust forcing from the same EMAC simulation excluding/including the dust-pollution interaction.

Table 1. Emission setups

Simulation	1	2	3	4
Anthropogenic emissions	yes	yes	no	no
Dust emissions	yes	no	yes	no